The metal-ion-dependent adhesion site in the Von Willebrand factor-A domain of $\alpha_2\delta$ subunits is key to trafficking voltage-gated Ca^{2+} channels

C. Cantí*, M. Nieto-Rostro*, I. Foucault*, F. Heblich*, J. Wratten, M. W. Richards, J. Hendrich, L. Douglas, K. M. Page, A. Davies, and A. C. Dolphin†

Department of Pharmacology, University College London, London WC1E 6BT, United Kingdom

Edited by William A. Catterall, University of Washington School of Medicine, Seattle, WA, and approved June 24, 2005 (received for review May 20, 2005)

All auxiliary $\alpha_2\delta$ subunits of voltage-gated Ca^{2+} (Ca_V) channels contain an extracellular Von Willebrand factor-A (VWA) domain that, in $\alpha_2\delta$-1 and -2, has a perfect metal-ion-dependent adhesion site (MIDAS). Modeling of the $\alpha_2\delta$-2 VWA domain shows it to be highly likely to bind a divalent cation. Mutating the three key MIDAS residues responsible for divalent cation binding resulted in a MIDAS mutant $\alpha_2\delta$-2 subunit that was still processed and trafficked normally when it was expressed alone. However, unlike WT $\alpha_2\delta$-2, the MIDAS mutant $\alpha_2\delta$-2 subunit did not enhance and, in some cases, further diminished $Ca_V1.2$, -2.1, and -2.2 currents coexpressed with β1b by using either Ba^{2+} or Na^+ as a permeant ion. Furthermore, expression of the MIDAS mutant $\alpha_2\delta$-2 reduced surface expression and strongly increased the perinuclear retention of $Ca_V\alpha$1 subunits at the earliest time at which expression was observed in both Cos-7 and NG108–15 cells. Despite the presence of endogenous $\alpha_2\delta$ subunits, heterologous expression of $\alpha_2\delta$-2 in differentiated NG108–15 cells further enhanced the endogenous high-threshold Ca^{2+} currents, whereas this enhancement was prevented by the MIDAS mutations. Our results indicate that $\alpha_2\delta$ subunits normally interact with the $Ca_V\alpha$1 subunit early in their maturation, before the appearance of functional plasma membrane channels, and an intact MIDAS motif in the $\alpha_2\delta$ subunit is required to promote trafficking of the α1 subunit to the plasma membrane by an integrin-like switch. This finding provides evidence for a primary role of a VWA domain in intracellular trafficking of a multimeric complex, in contrast to the more usual roles in binding extracellular ligands in other exofacial VWA domains.

integrin | neuron | motif | expression

Voltage-gated Ca^{2+} (Ca_V) channels are composed of a pore-forming α1 subunit that determines the main biophysical properties of the channel. For the Ca_V1 and -2 subfamilies, this subunit is associated with an intracellular β subunit (for review, see refs. 1 and 2) and a membrane-anchored, predominantly extracellular $\alpha_2\delta$ subunit (for review, see ref. 3). Mammalian genes encoding 10 α1, 4 β, and 4 $\alpha_2\delta$ subunits have been identified (for reviews, see refs. 2 and 4). The topology of the $\alpha_2\delta$ protein has been determined in detail only for $\alpha_2\delta$-1 but is thought to generalize to all 4 $\alpha_2\delta$ subunits (for review, see ref. 3). All $\alpha_2\delta$ subunits have predicted N-terminal signal sequences, indicating that the N terminus is extracellular. In early studies of $\alpha_2\delta$-1 purified from skeletal and cardiac muscle, it was determined that the α_2 subunit is disulfide-bonded to a transmembrane δ subunit, and both subunits are the products of a single gene, encoding the $\alpha_2\delta$ protein, that is posttranslationally cleaved into α_2 and δ (5).

Subsequent to the identification of $\alpha_2\delta$ subunits as stoichiometric components of skeletal muscle Ca^{2+} channels, $\alpha_2\delta$ subunits have also been shown to be associated with native cardiac (L-type) (6) and neuronal N- and P/Q-type channels (7, 8). In coexpression studies where it has been tested, all $\alpha_2\delta$ subunits enhance all Ca_V1 and -2 currents. The $\alpha_2\delta$ subunits also influence the channel's biophysical properties, including inactivation kinetics and voltage-dependence (9); therefore, the effects of the $\alpha_2\delta$ subunits are not limited to trafficking α1 subunits, but their mechanism of action remains largely unknown.

The $\alpha_2\delta$-1 subunit has been shown to bind to extracellular regions, including Domain III on $Ca_V\alpha$1 subunits (10, 11). It is unclear what domains of $\alpha_2\delta$ are involved in these interactions, but all $\alpha_2\delta$ subunits contain a Von Willebrand factor-A (VWA) domain within the α_2 moiety (12). This domain is also present in integrins and is often involved in binding extracellular matrix proteins (12, 13). VWA domains contain a sequence motif representing a metal-ion-dependent adhesion site (MIDAS) that confers divalent metal (usually Mg^{2+})-dependent binding to the ligand (14). In $\alpha_2\delta$-1 and -2, this motif is a perfect MIDAS motif, containing both the DxSxS motif and noncontiguous T and D residues (12), with the T in loop 3 being part of a TDG motif (15), suggesting that $\alpha_2\delta$-1 and -2 can both undergo an integrin-like switch and bind ligand in the presence of a divalent cation.

In this study, we have investigated the importance of the VWA domain MIDAS in the functional effects of $\alpha_2\delta$-2.

Experimental Procedures

Structural Modeling and CD. Suitable templates for modeling were selected from available structures by using the program FUGUE (16).

Construction and Heterologous Expression of cDNAs Cell Culture and Immunocytochemistry. Standard molecular biological and cell biological techniques were used, as described in refs. 17 and 18.

Biochemistry and Imaging. Cell-surface proteins in intact cells were biotinylated by using Sulfo-NHS-SS-Biotin (Pierce) for 30 min at room temperature. Standard techniques were used for immunoprecipitation, immunoblotting, and immunocytochemistry. Images were obtained by using a Zeiss LSM confocal microscope and further analyzed with IMAGEJ software (National Institutes of Health, Bethesda). The gabapentin-binding assay was performed by using a method similar to that described in ref. 19.

Electrophysiology. Standard techniques were used, essentially as described in ref. 17. Details are given in *Supporting Methods*, which is published as supporting information on the PNAS web site.

Further details of all methods are given in *Supporting Methods*. Data are mean (±SEM), and statistical significances were analyzed by using Student's *t* test for unpaired data.

This paper was submitted directly (Track II) to the PNAS office.

Abbreviations: Ca_V, voltage-gated Ca^{2+}; HVA, high-voltage-activated; I_{Ba}, Ba^{2+} current; MIDAS, metal-ion-dependent adhesion site; VWA, Von Willebrand factor-A.

*C.C., M.N.-R., I.F., and F.H. contributed equally to this work.

†To whom correspondence should be addressed at: Department of Pharmacology, University College London, Gower Street, London WC1E 6BT, United Kingdom. E-mail: a.dolphin@ucl.ac.uk.

www.pnas.org/cgi/doi/10.1073/pnas.0504183102

Results

Structural Modeling of the VWA Domain of $\alpha_2\delta$-2. Before investigating the function of the predicted VWA domain of $\alpha_2\delta$-2, we first determined the likelihood that $\alpha_2\delta$-2 is able to fold into a VWA domain. Suitable templates for modeling of $\alpha_2\delta$ VWA domains (residues 253–430 of $\alpha_2\delta$-1 and residues 294–472 of $\alpha_2\delta$-2) were selected from available structures. The 1.5-Å crystal structure of the VWA domain from capillary morphogenesis protein 2 (CMG2) in the open (ligand-competent) state and containing a Mg^{2+} ion in its MIDAS (20), was the best template for both $\alpha_2\delta$-1 and -2 VWA domains, with z scores of 15.62 and 18.85, respectively, indicating very high levels of certainty that this is an appropriate template structure. The pairwise sequence identity between each of the $\alpha_2\delta$ subunits and CMG2 is only ≈16% within the VWA region, but the residues of the MIDAS motif are conserved (see Fig. 6, which is published as supporting information on the PNAS web site). Models (Fig. 1*a*) were generated according to structural alignments, based on the CMG2 structure. A Mg^{2+} ion was replaced manually within the MIDAS.

Mutation of the MIDAS Residues of $\alpha_2\delta$-2 Do Not Prevent Its Trafficking, Processing Glycosylation, or Expression at the Cell Surface. The results of the modeling study encouraged us to examine the role of the VWA domain in $\alpha_2\delta$-2 by mutating to Ala the three divalent metal-coordinating amino acids D300, S302, and S304 in the MIDAS sequence DxSxS ($\alpha_2\delta$-2 μMIDAS, Fig. 1*b*). Mutation of MIDAS motifs in integrins has been used previously to probe the cell-surface role of ligand-binding to these sites (21). We found that mutation of the MIDAS motif did not affect the total expression levels of these constructs, compared with WT $\alpha_2\delta$-2, when transfected into tsA-201 (data not shown) or Cos-7 cells (Fig. 1*c*). In addition, $\alpha_2\delta$-2 μMIDAS was expressed at the cell surface in Cos-7 cells to the same extent as WT $\alpha_2\delta$-2, as determined by cell-surface biotinylation (Fig. 1*c*). The biotinylated $\alpha_2\delta$-2 and $\alpha_2\delta$-2 μMIDAS had the same molecular mass and were reduced in mass to the same extent by endoglycosidase F, suggesting that they are equally glycosylated (Fig. 1*d*). Cell-surface immunoreactivity in nonpermeabilized cells was observed for both constructs, with not only the anti-peptide α_2-2 (102–117) Ab (Fig. 1*e*) but also an Ab against amino acids in δ-2 (994–1009) (Fig. 1*e*). No increase in intracellular retention was observed for $\alpha_2\delta$-2 μMIDAS, compared with WT $\alpha_2\delta$-2 in permeabilized cells (Fig. 1*e*). Further evidence of the correct processing of $\alpha_2\delta$-2 μMIDAS is shown by the cleavage of its N-terminal signal peptide, because no surface staining was observed with the α_2-2 (16–29) signal peptide Ab for either construct (Fig. 1*e*), whereas extensive staining was observed in the perinuclear region in permeabilized cells (Fig. 1*e*).

It is unlikely, based on previous work on integrins (21), that mutation of MIDAS amino acids will cause the $\alpha_2\delta$-2 VWA domain to misfold, and, indeed, we have found that GST-fusion proteins of the WT and MIDAS mutant VWA domains of $\alpha_2\delta$-2 expressed and purified from *Escherichia coli* have very similar CD spectra. The model (Fig. 1*a*) predicts 40% α-helix, 22% β-sheet, and 38% other structure. The values obtained from CD measurements, after subtraction of the GST spectra, were 32%, 20%, and 48%, respectively [normalized root-mean-square deviation (NRMSD), 0.073], for the WT $\alpha_2\delta$-2 VWA domain and 31%, 23%, and 46% (NRMSD, 0.06) for the $\alpha_2\delta$-2 μMIDAS VWA domain. Furthermore, WT $\alpha_2\delta$-2 and $\alpha_2\delta$-2 μMIDAS exhibit similar affinity for binding of [^{3}H]gabapentin (K_D of 163.3 ± 8.7 nM and 166.1 ± 1.0 nM, respectively, $n = 3$ experiments), also indicative of correct folding of the full-length $\alpha_2\delta$-2 μMIDAS. The K_D for WT $\alpha_2\delta$-2 is in agreement with data published in ref. 19.

Effect of Mutation of the MIDAS Motif in the VWA Domain on Modulation of Ca^{2+}-Channel Currents by $\alpha_2\delta$-2. The amplitude of the very small Ba^{2+} currents (I_{Ba}) through $Ca_V2.2/\beta1b$ channels, expressed in tsA-201 cells, was enhanced ≈5-fold by WT $\alpha_2\delta$-2 (Fig. 2 *a–c*) and by $\alpha_2\delta$-2 with a C-terminal myc-His tag (Fig. 2*a*). In contrast, $\alpha_2\delta$-2 μMIDAS produced no stimulation of $Ca_V2.2$ currents (Fig. 2 *a* and *b*). Furthermore, steady-state inactivation was slightly hyperpolarized by $\alpha_2\delta$-2, with an increase in voltage-dependence compared with the $Ca_V2.2/\beta1b$ combination, but

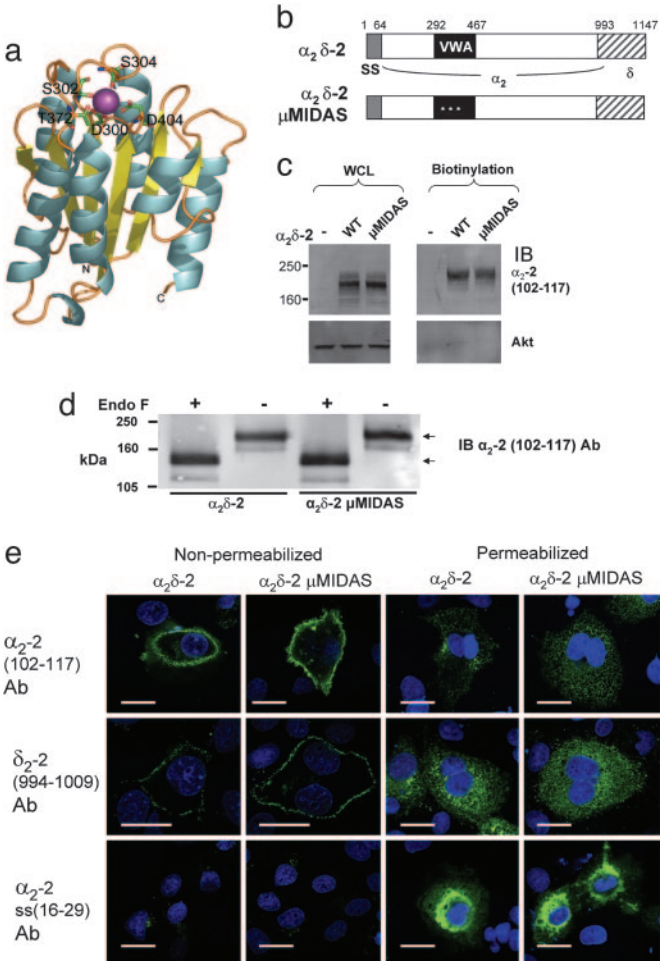

Fig. 1. Mutation of the MIDAS in $\alpha_2\delta$-2 does not prevent its trafficking to the plasma membrane. (*a*) Model of the $\alpha_2\delta$-2 VWA domain. Residues comprising the MIDAS motif are labeled and shown as stick representations. The Mg^{2+} ion (purple) is coordinated within the MIDAS and is partially exposed at the surface in an appropriate manner for interaction with a second protein. α-helices are colored in cyan and β-strands in yellow. (*b*) The main domains in the primary sequence of $\alpha_2\delta$-2, showing the extent of the VWA domain (black), and the three MIDAS mutations (white asterisks). SS, signal sequence. The amino acids making up the δ subunit are indicated by hatched boxes. (*c*) Cos-7 cells were transfected with either $\alpha_2\delta$-2 or $\alpha_2\delta$-2 μMIDAS, as indicated, and cell-surface proteins were biotinylated. (*Left*) Total expression in whole-cell lysate (WCL). (*Right*) Pull-down of biotinylated proteins on a 3–8% Tris acetate gel. (*Upper*) α_2-2 (residues 102–117) Ab was used for immunoblotting (IB). (*Lower*) Anti-Akt Ab was used for IB to show that no intracellular proteins were biotinylated. The percentages of $\alpha_2\delta$-2 and $\alpha_2\delta$-2 μMIDAS at the cell surface were 10.0% and 9.5%, respectively (representative of three independent experiments; see Fig. 9 legend for calculation details). (*d*) Biotinylated $\alpha_2\delta$-2 (*Left*) or $\alpha_2\delta$-2 μMIDAS (*Right*), as in *c*, were treated (+) or not (−) with endoglycosidase F (5 units) and separated on a 7% Tris acetate gel. The upper arrow indicates fully glycosylated $\alpha_2\delta$-2, and the lower arrow indicates deglycosylated $\alpha_2\delta$-2. (*e*) Localization of $\alpha_2\delta$-2 and $\alpha_2\delta$-2 μMIDAS 48 h after transfection in Cos-7 cells that were either nonpermeabilized (*Left*) or permeabilized (*Right*) before immunostaining with the primary Abs shown. (*Top*) α_2-2 (residues 102–117) Ab. (*Middle*) δ_2-2(residues 994-1009)Ab. (*Bottom*) Signal peptide α_2-2 (residues 16–29) Ab. (Scale bar, 20 μm.)

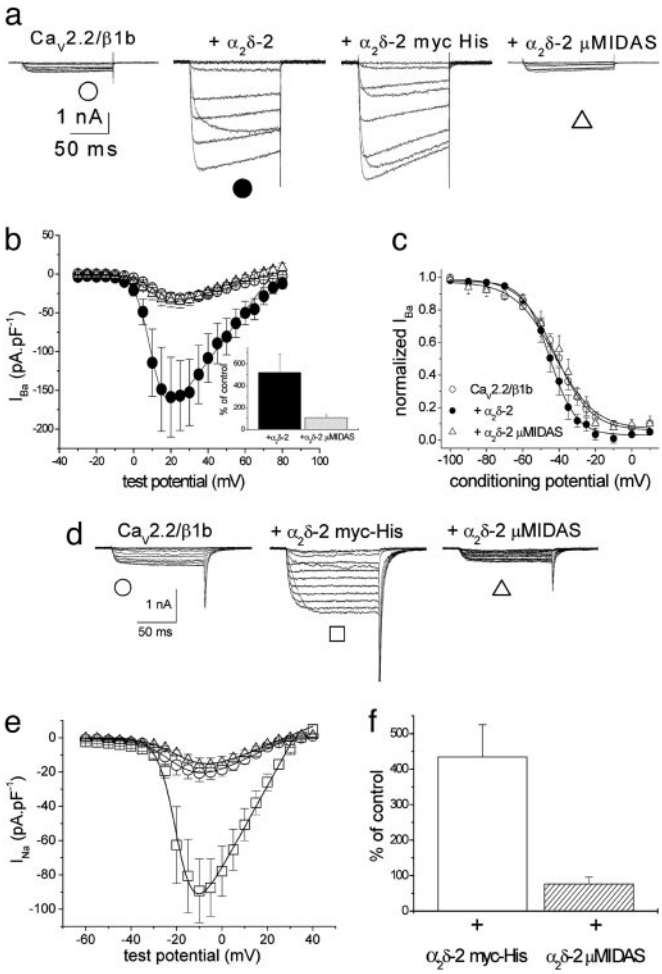

Fig. 2. Comparison of the effect of $\alpha_2\delta$-2 and the MIDAS mutant construct of $\alpha_2\delta$-2 on Ca_V currents in tsA-201 cells. $Ca_V2.2/\beta1b$ was expressed with the various $\alpha_2\delta$-2 constructs in tsA-201 cells by using 10 mM Ba^{2+}as charge carrier (see *Supporting Methods*). (*a*) Representative current traces elicited between −20 and +40 mV in 10-mV steps from a holding potential (HP) of −90 mV for $Ca_V2.2/\beta1b$ (*Left*), $Ca_V2.2/\beta1b/\alpha_2\delta$-2 (*Center Left*), $Ca_V2.2/\beta1b/\alpha_2\delta$-2 myc-His (*Center Right*), and $Ca_V2.2/\beta1b/\alpha_2\delta$-2 μMIDAS (Right). (*b*) Current–voltage (*I–V*) relationships for three of the experimental conditions. ○, $Ca_V2.2/\beta1b$ ($n = 8$); ●, $+\alpha_2\delta$-2 ($n = 10$); and △, $+\alpha_2\delta$-2 μMIDAS ($n = 11$). (*Inset*) Bar chart at +20 mV (calculated as a percentage of the mean control $Ca_V2.2/\beta1b$ currents) for $+\alpha_2\delta$-2 (back bar) and $+\alpha_2\delta$-2 μMIDAS (hatched bar). The number of determinations is as described above. (*c*) Steady-state inactivation curves for test pulses to +20 mV from a 15-s conditioning prepulse of between −100 and 0 mV. ○, $Ca_V2.2/\beta1b$ ($n = 9$); ●, $+\alpha_2\delta$-2 ($n = 7$); and △, $+\alpha_2\delta$-2 μMIDAS ($n = 5$). The data were fit with a single Boltzmann equation and the mean voltages at which the channel is 50% available (V_{50}) for inactivation were −42.4, −45.9, and −42.0 mV, respectively, and the slope factors (*k*) were 11.1, 7.2, and 9.8 mV, respectively. (*d*) $Ca_V2.2/\beta1b$ was expressed with the various $\alpha_2\delta$-2 constructs and 100 mM Na^+ was used as charge carrier (see *Supporting Methods*). Representative current traces were elicited between −40 and +15 mV in 5-mV steps from a holding potential of −90 mV for $Ca_V2.2/\beta1b$ (*Left*), $Ca_V2.2/\beta1b/\alpha_2\delta$-2 myc-His (*Center*), and $Ca_V2.2/\beta1b/\alpha_2\delta$-2 μMIDAS (*Right*). (*e*) *I–V* relationships for the three conditions. ○, $Ca_V2.2/\beta1b$ ($n = 16$); □, $+\alpha_2\delta$-2 myc-His ($n = 17$); and △, $+\alpha_2\delta$-2 μMIDAS ($n = 15$). (*f*) Bar chart at −10 mV (calculated as a percentage of the mean control $Ca_V2.2/\beta1b$ Na^+ currents) for $+\alpha_2\delta$-2 myc-His (open bar) and $+\alpha_2\delta$-2 μMIDAS (hatched bar). The number of determinations is as in *e*.

this effect did not occur for $\alpha_2\delta$-2 μMIDAS (Fig. 2*c*). A similar result was obtained by using HA-tagged $Ca_V1.2$ (22) (see Fig. 7 *a–c*, which is published as supporting information on the PNAS web site). In cerebellar Purkinje cells, we have shown that $\alpha_2\delta$-2 is the predominant $\alpha_2\delta$ subtype (17), and, here, the main $\alpha1$ and β subunits are $Ca_V2.1$ and $\beta4$ (23, 24). We therefore compared the effect of $\alpha_2\delta$-2 and $\alpha_2\delta$-2 μMIDAS on $Ca_V2.1/\beta4$ currents. Whereas $\alpha_2\delta$-2 enhanced the $Ca_V2.1/\beta4$ current by 6.8-fold ± 0.6 ($n = 10$), there was no significant effect of $\alpha_2\delta$-2 μMIDAS (data not shown).

In *Xenopus* oocytes, the amplitude of $Ca_V2.2/\beta1b$ currents was enhanced ≈3-fold by both WT $\alpha_2\delta$-2 and $\alpha_2\delta$-2 myc-His (see Fig. 7 *d* and *e*). In contrast, after mutation of the MIDAS amino acids, there was no enhancement of the current amplitude, and, indeed, there was a clear reduction, compared with $Ca_V2.2/\beta1b$ alone (see Fig. 7 *d* and *e*). Furthermore, whereas $\alpha_2\delta$-2 hyperpolarized the voltage-dependence of steady-state inactivation, $\alpha_2\delta$-2 μMIDAS did not (see Fig. 7*f*). All data obtained with $\alpha_2\delta$-2 μMIDAS could be replicated by using an $\alpha_2\delta$-2 construct in which the VWA domain was deleted (data not shown).

We detected no endogenous $\alpha_2\delta$ subunit protein in *Xenopus* oocytes (see Fig. 8*a*, which is published as supporting information on the PNAS web site) or Cos-7 cells (data not shown), whereas endogenous $\alpha_2\delta$-1 was detected in tsA-201 cells. The $\alpha_2\delta$-1 had the same molecular mass and was glycosylated to the same extent as was $\alpha_2\delta$-1 in brain (see Fig. 8*b*). No endogenous $\alpha_2\delta$-2 was observed in any of the cell types used (data not shown).

Does the Effect of Mutation of the MIDAS on Ca^{2+}-Channel Currents Involve Binding of Extracellular Divalent Cations? Because MIDAS motifs bind divalent cations (Fig. 1*a*), we wished to examine whether the effect of mutation of the MIDAS affected channel permeation. We therefore removed all divalent cations from the external medium and measured Na^+ flux through $Ca_V2.2$ channels in tsA-201 cells. This protocol produced the same result: the amplitude of the $Ca_V2.2/\beta1b$ Na^+ currents was enhanced >4-fold by $\alpha_2\delta$-2 but not by $\alpha_2\delta$-2 μMIDAS, whose currents were slightly smaller than those in the absence of any $\alpha_2\delta$-2 (Fig. 2 *d–f*). Therefore, if Mg^{2+} (or Ca^{2+}) binding to the MIDAS in $\alpha_2\delta$-2 is involved in its function in relation to enhancing currents through $Ca_V\alpha1$ channels, it must be during the process of channel assembly or trafficking rather than during the permeation process, once the channels have reached the cell surface.

Does the MIDAS Mutant $\alpha_2\delta$-2 Affect Trafficking of $Ca_V\alpha1$ Subunits? Given these results, the complete loss of function of the $\alpha_2\delta$-2 μMIDAS mutant subunit, despite its normal expression compared with WT $\alpha_2\delta$-2, might, therefore, be due to interference with trafficking and a subsequent reduction of plasma-membrane expression of associated $Ca_V\alpha1$ subunits. Using cell surface biotinylation, we found a decrease in the percentage of $Ca_V2.2$ at the cell surface, when coexpressed with $\alpha2\delta$-2 μMIDAS, compared with WT $\alpha_2\delta$-2 by ≈50% (see Fig. 9*a*, which is published as supporting information on the PNAS web site) and also a 30% decrease in the percentage of $\alpha2\delta$-2 μMIDAS, compared with WT $\alpha_2\delta$-2 at the cell surface, when coexpressed with $Ca_V2.2$ (see Fig. 10*b*, which is published as supporting information on the PNAS web site). This result was not the case when the $\alpha_2\delta$ subunits were expressed alone (Fig. 1*c*).

To examine further the basis for the reduction of surface expression of $Ca_V\alpha1$ subunits, we determined the subcellular distribution of HA-$Ca_V1.2$, expressed with $\beta1b$ in Cos-7 cells in the presence of either $\alpha_2\delta$-2 or $\alpha_2\delta$-2 μMIDAS. When HA-$Ca_V1.2$ was expressed with WT $\alpha_2\delta$-2, its distribution was fairly uniform (Fig. 3*a*; and see Fig. 10 for an additional example). The immunostaining extended to the periphery of the cell, where it colocalized with $\alpha_2\delta$-2, as seen clearly on the line scan (representative of 11 of 11 cells analyzed in three experiments, see Fig. 3*b*). Further evidence of colocalization was obtained from pixel-intensity-correlation plots (Fig. 3*c*).

In contrast, when HA-$Ca_V1.2$ was coexpressed with $\alpha_2\delta$-2 μMIDAS, areas of marked intracellular retention were observed, most often of both the $Ca_V\alpha1$ and the $\alpha_2\delta$ subunit (Fig.

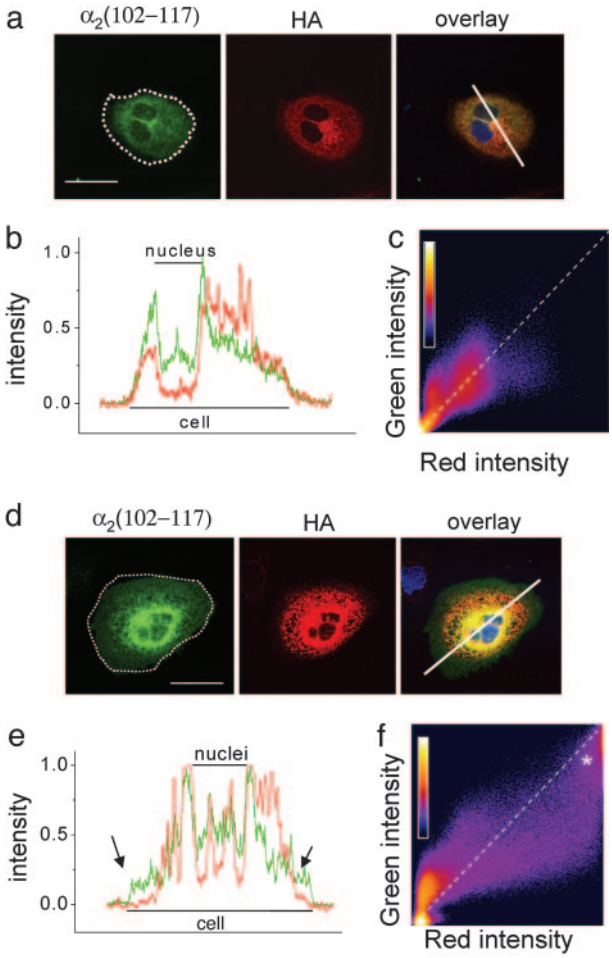

Fig. 3. Comparison of the effect of $\alpha_2\delta$-2 and $\alpha_2\delta$-2 μMIDAS on expression of $Ca_V1.2$ channels and colocalization with the $\alpha_2\delta$ construct. (*a* and *d*) Localization of $\alpha_2\delta$-2 or $\alpha_2\delta$-2 μMIDAS (α_2 (102–117) Ab (*Left*), cell outline shown by dotted white line), HA-$Ca_V1.2$ (HA Ab, *Center*), and overlay (*Right*), including nuclear stain (DAPI, blue) in $Ca_V1.2/\beta1b/\alpha_2\delta$-2 (*a*) or $\alpha_2\delta$-2 μMIDAS-transfected Cos-7 cells (*d*). (Scale bar, 50 μm.) (*b* and *e*) Normalized pixel intensity of the line scan given on the image. The red line is HA-$Ca_V1.2$, and the green line is $\alpha_2\delta$-2 (*b*) or $\alpha_2\delta$-2 μMIDAS (*e*). The arrows in *e* indicate regions where $Ca_V1.2$ immunoreactivity is absent from the periphery of the cell. (*c* and *f*) Pixel-intensity-correlation plot for nonzero pixels in the entire image, shown for $\alpha_2\delta$-2 (*c*) or $\alpha_2\delta$-2 μMIDAS (*f*) (green, *y* axis) vs. $Ca_V1.2$ (red, *x* axis). A pixel-number calibration bar is shown on each plot. * in *f* indicates an additional region of high-intensity colocalization. The diagonal dotted line indicates theoretical colocalization. (*a–c*) Cos-7 cells HA-$Ca_V1.2/\beta1b/\alpha_2\delta$-2. (*d–f*) HA-$Ca_V1.2/\beta1b/\alpha_2\delta$-2 μMIDAS.

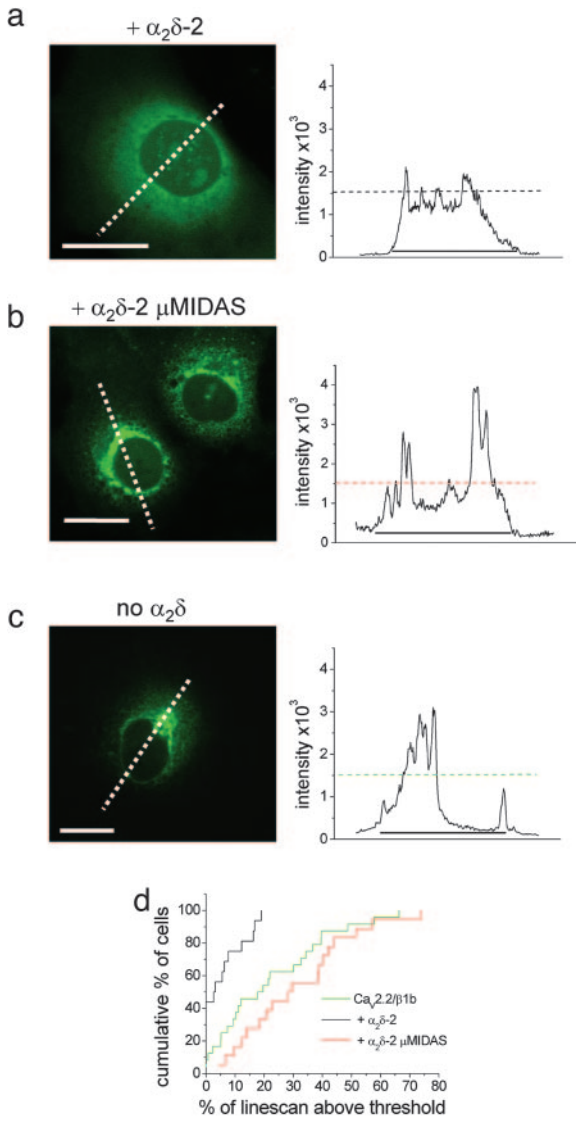

Fig. 4. Comparison of the effects of $\alpha_2\delta$-2 and $\alpha_2\delta$-2 μMIDAS on the distribution of GFP-$Ca_V2.2$ channels in Cos-7 cells. (*Left*) Localization of GFP-$Ca_V2.2$ in Cos-7 cells when coexpressed with $\beta1b$ and either $\alpha_2\delta$-2 (*a*) or $\alpha_2\delta$-2 μMIDAS (*b*) and without $\alpha_2\delta$ (*c*) 24 h after transfection. White dotted lines correspond to the positions of the line scans shown to the right. (Scale bars, 20 μm.) (*Right*) Line scans of GFP-$Ca_V2.2$ fluorescence were analyzed through the nucleus of the cells shown. The horizontal dotted lines show the 1,500 intensity threshold (12-bit images), and the line beneath the scans shows the extent of the cell. (*d*) Cumulative frequency histogram of the percentage of the line scan within the cell above the 1,500 intensity threshold for $\alpha_2\delta$-2- ($n = 26$, black line), $\alpha_2\delta$-2 μMIDAS-containing cells ($n = 32$, red line), and in the absence of $\alpha_2\delta$ ($n = 32$, green line). The histogram shows the greater proportion of high-intensity GFP-$Ca_V2.2$ fluorescence regions in $\alpha_2\delta$-2 μMIDAS (mean 33.2 $\pm$ 3.1%), compared with both $\alpha_2\delta$-2-containing cells (mean 10.1 $\pm$ 2.4%; $P < 0.0001$) and in the absence of $\alpha_2\delta$ (mean 21.2 $\pm$ 3.2%; $P < 0.01$, compared with $\alpha_2\delta$-2 μMIDAS).

3*d*; and see Fig. 10 for an additional example). Furthermore, in 9 of 14 cells examined, HA-$Ca_V1.2$ immunoreactivity was observed not to extend as far as $\alpha_2\delta$-2 μMIDAS into the periphery of the cell (Fig. 3*e*). The strong intracellular retention of HA-$Ca_V1.2$, together with $\alpha_2\delta$-2 μMIDAS, can be seen clearly on the pixel-intensity-correlation plot as an additional peak of high intensity in both red and green fluorescence (Fig. 3*f*, marked with an asterisk). In agreement with these results, HA-$Ca_V1.2$ is able to coimmunoprecipitate with $\alpha_2\delta$-2 μMIDAS and WT $\alpha_2\delta$-2 (Fig. 9*c*).

We then used an N-terminal GFP-$Ca_V2.2$ construct, which we have previously shown exhibits normal functional properties in Cos-7 cells (25). We examined expression at a very early time point, 24 h after transfection, before the time at which Ca^{2+} currents could reliably be recorded (data not shown). Compared with coexpression with WT $\alpha_2\delta$-2, where the distribution of GFP-$Ca_V2.2$ was fairly uniform, when coexpressed with $\alpha_2\delta$-2 μMIDAS, there was a significantly greater intracellular accumulation of GFP-$Ca_V2.2$, particularly in the perinuclear region (Fig. 4 *a*, *b*, and *d*). The accumulation was also more pronounced than that seen with GFP-$Ca_V2.2$, in the absence of any $\alpha_2\delta$ (Fig. 4 *c* and *d*). The same result was observed 48 h after transfection (see Fig. 11, which is published as supporting information on the PNAS web site).

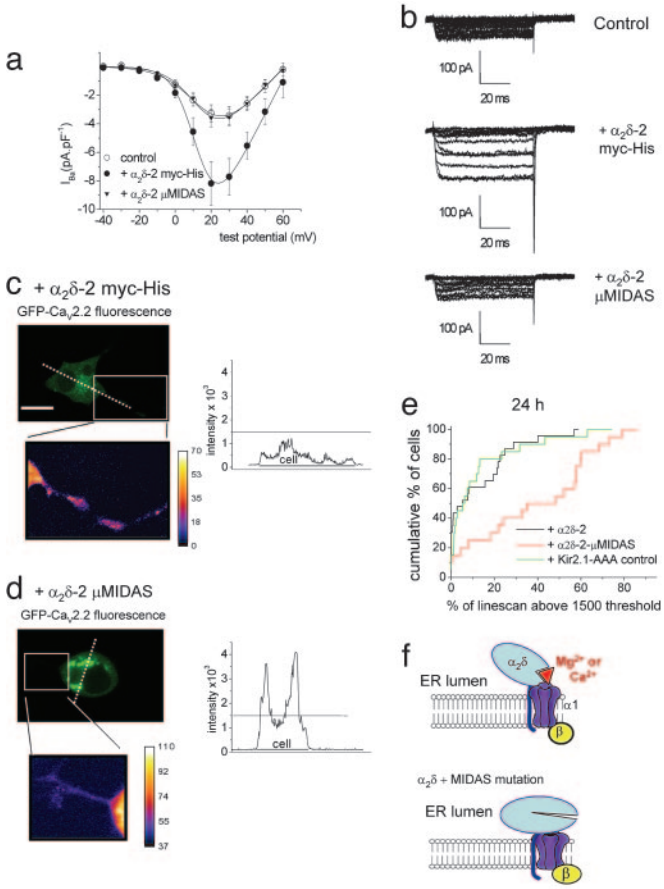

Fig. 5. Comparison of the effects of $\alpha_2\delta$-2 and $\alpha_2\delta$-2 μMIDAS on endogenous Ca^{2+} currents and GFP-Ca_V2.2 distribution in NG 108–15 cells. (*a*) The effects of $\alpha_2\delta$-2 and $\alpha_2\delta$-2 μMIDAS on HVA I_{Ba} in NG108–15 cells. Current–voltage relationships for NG108–15 cells transfected with GFP-pRK5 and Kir2.1-AAA (○, control, $n = 13$), ●, $\alpha_2\delta$-2 myc-His ($n = 12$), or ▼, $\alpha_2\delta$-2 μMIDAS ($n = 13$), all in pcDNA3.1. Holding potential = −40 mV. (*b*) Sample traces for the three conditions shown in *a*. (*Top*) Control. (*Middle*) +$\alpha_2\delta$-2. (*Bottom*) +$\alpha_2\delta$-2 μMIDAS. Traces shown are from −40 to +60 mV. (*c* and *d*) Localization of GFP-Ca_V2.2 48 h after transfection, cotransfected with β1b and $\alpha_2\delta$-2 myc-His (*c*) or $\alpha_2\delta$-2 μMIDAS (*d*). (*Top Left*) GFP fluorescence. (*Top Right*) Line scan of the dotted line shown on the 12-bit image. (*Bottom Left*) Enlarged region shown by the box, converted to 8-bit pseudocolor to show intensity in the neurite. The intensity calibration bars are shown on the right. (*e*) The plots represent a cumulative frequency histogram for all line scans, obtained 24 h after transfection, showing the significantly greater percentage of high-intensity GFP-Ca_V2.2-fluorescence regions in $\alpha_2\delta$-2 μMIDAS-containing cells (red line, mean 42.2 ± 6.1%, $n = 20$, $P < 0.0005$) in comparison with $\alpha_2\delta$-2-containing cells (black line, 14.6 ± 3.7%, $n = 23$). An additional control is included, in which a control nonfunctional protein, Kir2.1-AAA, has been included instead of $\alpha_2\delta$-2 (green, 15.6 ± 4.8%, $n = 20$, $P < 0.001$, compared with $\alpha_2\delta$-2 μMIDAS). (*f*) Proposed role of the MIDAS in $\alpha_2\delta$. ER, endoplasmic reticulum.

Effect of $\alpha_2\delta$-2 and $\alpha 2\delta$-2 μMIDAS on Expression of Ca^{2+}-Channel Currents in Differentiated NG108–15 Cells. The NG108–15 neuroblastoma–glioma hybrid cell line represents a model for neurons, because it produces extensive neurites and shows high-voltage-activated (HVA) currents, when differentiated. These currents were isolated by maintaining a holding potential of −40 mV. Despite the presence of endogenous $\alpha_2\delta$-1 in NG108–15 cells (26), exogenous expression of $\alpha_2\delta$-2 enhanced the HVA currents substantially. I_{Ba} recorded from differentiated cells transfected with $\alpha_2\delta$-2, was increased to 264% of control (Fig. 5 *a* and *b*), indicating that the amount of endogenous $\alpha 2\delta$ is suboptimal for the expression of maximal endogenous Ca^{2+} currents. In contrast, transfection with $\alpha_2\delta$-2 μMIDAS produced no enhancement of I_{Ba} (110% of control, Fig. 5 *a* and *b*).

When NG108–15 cells were transfected with GFP-Ca_V2.2/β1b and WT $\alpha_2\delta$-2 and differentiated, uniform distribution of GFP-Ca_V2.2 was observed (Fig. 5*c*). The cells were clearly differentiated with neurites (Fig. 5*d*, enlarged region). In sharp contrast, coexpression with $\alpha_2\delta$-2 μMIDAS produced strong perinuclear retention of GFP-Ca_V2.2/β1b, although the cells also had a differentiated phenotype, showing neurites (Fig. 5*d*). Analysis of the amount of signal above an arbitrary threshold on line scans (Fig. 5 *c* and *d*) showed that the intracellular retention of GFP-Ca_V2.2/β1b was significantly greater in the presence of $\alpha_2\delta$-2 μMIDAS than in the presence of WT $\alpha_2\delta$-2, at both 48 h (data not shown) and 24 h (Fig. 5*e*). In an additional control experiment, coexpression of GFP-Ca_V2.2/β1b with a control transmembrane protein Kir2.1-AAA (27), a K^+ channel with a mutation in the pore, such that it does not conduct current, does not produce any intracellular retention of Ca_V2.2/β1b (Fig. 5*e*). We also showed that GFP-Ca_V2.2 was expressed similarly under all conditions (see Fig. 12, which is published as supporting information on the PNAS web site).

Discussion

The Functional Interaction of $Ca_V\alpha 1/\beta$ Channels with $\alpha_2\delta$-2. Previous *in vitro* studies have shown that all $\alpha_2\delta$ subunits increase the maximum conductance of a number of expressed Ca^{2+}-channel $\alpha 1/\beta$ subunit combinations at the whole-cell level (1, 17, 28–30). We have previously investigated the effect of $\alpha_2\delta$-2 on the Ca_V2.1/β4 Ca^{2+}-channel subunit combination and showed that it had no effect on single-channel conductance (17, 18). This finding implies that $\alpha_2\delta$-2 probably has its main effect on the lifetime of the channel complex in the plasma membrane, by either enhancing forward trafficking or reducing turnover of the channel once inserted in the plasma membrane.

All integrin β subunits contain a VWA domain with a MIDAS motif (13). Based on structural studies, the inactive form of the integrin dimer is bent in a loose hairpin. When activated, the integrin dimers alter conformation and bind their ligands in the presence of divalent cations (usually Mg^{2+}, see Fig. 1*a*; for review, see ref. 31). The single particle EM studies of Ca^{2+}-channel complexes have also shown the associated $\alpha_2\delta$ subunit to be bent (32–34). It was recently hypothesized that all VWA domains that contain a perfect MIDAS motif (DxSxS and a coordinating T and D) will both bind Mg^{2+} and subsequently undergo an integrin-like switch (15). It is tempting to speculate that the $Ca_V\alpha 1$ subunit represents an endogenous ligand for the $\alpha_2\delta$ MIDAS and that an integrin-like switch is required for trafficking the channel complex.

Mechanism of Inhibition of Trafficking by the MIDAS Mutant of $\alpha_2\delta$-2. One hypothesis for the role of $\alpha_2\delta$ subunits is that they act as vestibules to increase Ca^{2+} availability at the mouth of the pore (35), and, therefore, mutating the MIDAS so that this motif is nonfunctional might reduce the conductance. If this were the mechanism, the effect should be lost when using Na^+ as the charge carrier. However, we have shown that exactly the same effect of $\alpha_2\delta$-2 μMIDAS occurs under these conditions as in the presence of divalent cations.

This finding leaves two further hypotheses. First, correct binding of a divalent cation to the $\alpha_2\delta$ MIDAS in the lumen of the endoplasmic reticulum or other intracellular compartment may be essential for the trafficking of $Ca_V\alpha 1$ subunits to the plasma membrane. Several pieces of our evidence support this hypothesis, pointing to a defect in $Ca_V\alpha 1$-subunit trafficking in the presence of $\alpha_2\delta$-2 μMIDAS, caused by an intracellular interaction between the two proteins. We observed marked intracellular retention of HA-Ca_V1.2 and intracellular colocalization with $\alpha_2\delta$-2 μMIDAS, whereas when $\alpha_2\delta$-2 μMIDAS is expressed alone, it is processed and trafficked to the cell membrane normally. A similar phenom-

enon of intracellular retention was observed for GFP-$Ca_V2.2$ in live Cos-7 and NG108–15 cells. We have also observed less $Ca_V2.2$ at the plasma membrane by cell-surface biotinylation when $\alpha_2\delta$-2 μMIDAS is coexpressed, compared with WT $\alpha_2\delta$-2. There was also a smaller proportion of $\alpha_2\delta$-2 μMIDAS at the cell surface when this subunit is coexpressed with $Ca_V2.2$, compared with when it is expressed alone, whereas this was not the case for WT $\alpha_2\delta$-2.

The second hypothesis would be that the $Ca_V\alpha1/\beta$ heterodimers and the $\alpha_2\delta$ subunits are trafficked separately to the plasma membrane, where they then interact, allowing the $\alpha_2\delta$ to increase the lifetime of the channel at the plasma membrane. A prediction based on this hypothesis is that there would be no interaction in the case of $\alpha_2\delta$-2 μMIDAS. Evidence against this hypothesis is (*i*) that the colocalization and coimmunoprecipitation of $\alpha_2\delta$-2 μMIDAS and $Ca_V\alpha1$ subunits indicates an interaction, albeit an abortive one, and (*ii*) that the intracellular retention of GFP-$Ca_V2.2$ was more marked in the presence of $\alpha_2\delta$-2 μMIDAS than in the absence of any $\alpha_2\delta$ subunit, before the time at which Ca^{2+} currents could be recorded, indicating that an interaction must occur early in the process of assembly and trafficking. Thus, even in the absence of a functional MIDAS in $\alpha_2\delta$-2, an interaction occurs, presumably through the mutated VWA domain and, possibly, through other sites in $\alpha_2\delta$-2, but this interaction does not result in trafficking. We propose that the interaction between $Ca_V\alpha1$ and an $\alpha_2\delta$ subunit requires the high divalent cation concentration within the endoplasmic reticulum (ER) to bind to the MIDAS in $\alpha_2\delta$ and allow forward trafficking of the complex through an integrin-like switch (Fig. 5*F*). This switch may serve as a trafficking checkpoint, so that, if the $Ca_V\alpha1$ subunit is not folded correctly, both $\alpha1$ and $\alpha_2\delta$ will be retained within the ER.

Mechanism of Suppression of $Ca_V\alpha1$ Currents by MIDAS Mutant $\alpha_2\delta$-2. There is a strong suppressive effect of $\alpha_2\delta$-2 μMIDAS in *Xenopus* oocytes, whereas in NG108–15 cells and tsA 201 cells, only a lack of up-regulation of the endogenous HVA I_{Ba} by $\alpha_2\delta$-2 μMIDAS is seen. The clear difference that we have found between these expression systems is the presence of endogenous $\alpha_2\delta$-1 in NG108–15 cells (26) and in tsA 201 cells, whereas no endogenous $\alpha_2\delta$ protein was detected in the *Xenopus* oocytes used in this study (Fig. 7). We therefore suggest that, in *Xenopus* oocytes, in the absence of any endogenous $\alpha_2\delta$ subunits, $\alpha_2\delta$-2 μMIDAS interacts with, and causes intracellular retention of, expressed $Ca_V\alpha1/\beta$ complexes, which otherwise produce substantial currents in this system, although not in mammalian cells, for reasons unknown (e.g., Fig. 2 *a–c*, compared with Fig. 7 *d* and *e*). In contrast, the channels underlying the very small $Ca_V\alpha1/\beta$ I_{Ba} observed in tsA 201 cells may reach the plasma membrane only because they have an associated endogenous $\alpha_2\delta$. Furthermore, in NG108–15 cells, there is evidence that the up-regulation of endogenous Ca^{2+} currents that occurs upon differentiation results, at least in part, from the stabilization of preformed channels (36), and, thus, the channels making up the endogenous HVA current in NG108–15 cells are likely to already have an associated endogenous $\alpha_2\delta$-1. These endogenous channels would, therefore, be protected from association with the MIDAS mutant of $\alpha_2\delta$-2 and, thus, from further suppression by intracellular retention.

Conclusions

Our finding that $\alpha_2\delta$-2 μMIDAS increased the internal retention of both Ca_V1 and Ca_V2 channels, whereas it is normally processed and trafficked itself when expressed alone, indicates that the MIDAS motif of the VWA domain has its action on trafficking of the $Ca_V\alpha1$ subunit. Our results suggest that $\alpha_2\delta$ subunits normally interact, through the intact MIDAS, with the $Ca_V\alpha1$ subunit at a very early time point in their maturation, to enhance trafficking. This finding provides evidence for a primary role of a VWA domain in the intracellular trafficking of a multimeric complex, in contrast to their more usual role in extracellular interactions.

We thank Dr. E. Bourinet (Institut de Génétique Humaine–Centre National de la Recherche Scientifique, Montpellier, France) for HA-tagged $Ca_V1.2$ cDNA and Dr. W. J. Frith for help with image processing. This work was supported, in part, by the Medical Research Council (United Kingdom) and the Wellcome Trust.

1. Walker, D. & De Waard, M. (1998) *Trends Neurosci.* **21,** 148–154.
2. Dolphin, A. C. (2003) *J. Bioeng. Biomembr.* **35,** 599–620.
3. Arikkath, J. & Campbell, K. P. (2003) *Curr. Opin. Neurobiol.* **13,** 298–307.
4. Catterall, W. A. (2000) *Annu. Rev. Cell Dev. Biol.* **16,** 521–555.
5. Jay, S. D., Sharp, A. H., Kahl, S. D., Vedvick, T. S., Harpold, M. M. & Campbell, K. P. (1991) *J. Biol. Chem.* **266,** 3287–3293.
6. Chang, F. C. & Hosey, M. M. (1988) *J. Biol. Chem.* **263,** 18929–18937.
7. Witcher, D. R., De Waard, M., Sakamoto, J., Franzini-Armstrong, C., Pragnell, M., Kahl, S. D. & Campbell, K. P. (1993) *Science* **261,** 486–489.
8. Liu, H., De Waard, M., Scott, V. E. S., Gurnett, C. A., Lennon, V. A. & Campbell, K. P. (1996) *J. Biol. Chem.* **271,** 13804–13810.
9. Canti, C., Davies, A. & Dolphin, A. C. (2003) *Curr. Neuropharmacol.* **1,** 209–217.
10. Felix, R., Gurnett, C. A., De Waard, M. & Campbell, K. P. (1997) *J. Neurosci.* **17,** 6884–6891.
11. Gurnett, C. A., Felix, R. & Campbell, K. P. (1997) *J. Biol. Chem.* **272,** 18508–18512.
12. Whittaker, C. A. & Hynes, R. O. (2002) *Mol. Biol. Cell* **13,** 3369–3387.
13. Humphries, M. J. (2000) *Biochem. Soc. Trans.* **28,** 311–340.
14. Plow, E. F., Haas, T. K., Zhang, L., Loftus, J. & Smith, J. W. (2000) *J. Biol. Chem.* **275,** 21785–21788.
15. Bhattacharya, A. A., Lupher, M. L., Jr., Staunton, D. E. & Liddington, R. C. (2004) *Structure (Cambridge, U.K.)* **12,** 371–378.
16. Shi, J., Blundell, T. L. & Mizuguchi, K. (2001) *J. Mol. Biol.* **310,** 243–257.
17. Barclay, J., Balaguero, N., Mione, M., Ackerman, S. L., Letts, V. A., Brodbeck, J., Canti, C., Meir, A., Page, K. M., Kusumi, K., *et al.* (2001) *J. Neurosci.* **21,** 6095–6104.
18. Brodbeck, J., Davies, A., Courtney, J.-M., Meir, A., Balaguero, N., Canti, C., Moss, F. J., Page, K. M., Pratt, W. S., Hunt, S. P., *et al.* (2002) *J. Biol. Chem.* **277,** 7684–7693.
19. Marais, E., Klugbauer, N. & Hofmann, F. (2001) *Mol. Pharmacol.* **59,** 1243–1248.
20. Lacy, D. B., Wigelsworth, D. J., Scobie, H. M., Young, J. A. & Collier, R. J. (2004) *Proc. Natl. Acad. Sci. USA* **101,** 6367–6372.
21. Chen, J., Salas, A. & Springer, T. A. (2003) *Nat. Struct. Biol.* **10,** 995–1001.
22. Altier, C., Dubel, S. J., Barrère, C., Jarvis, S. E., Stotz, S. C., Spaetgens, R. L., Scott, J. D., Cornet, V., De Waard, M., Zamponi, G. W., *et al.* (2002) *J. Biol. Chem.* **277,** 33598–33603.
23. Fletcher, C. F., Lutz, C. M., O'Sullivan, T. N., Shaughnessy, J. D., Jr., Hawkes, R., Frankel, W. N., Copeland, N. G. & Jenkins, N. A. (1996) *Cell* **87,** 607–617.
24. Burgess, D. L., Jones, J. M., Meisler, M. H. & Noebels, J. L. (1997) *Cell* **88,** 385–392.
25. Raghib, A., Bertaso, F., Davies, A., Page, K. M., Meir, A., Bogdanov, Y. & Dolphin, A. C. (2001) *J. Neurosci.* **21,** 8495–8504.
26. Wyatt, C. N., Page, K. M., Berrow, N. S., Brice, N. L. & Dolphin, A. C. (1998) *J. Physiol. (London)* **510,** 347–360.
27. Tinker, A., Jan, Y. N. & Jan, L. Y. (1996) *Cell* **87,** 857–868.
28. Mori, Y., Friedrich, T., Kim, M.-S., Mikami, A., Nakai, J., Ruth, P., Bosse, E., Hofmann, F., Flockerzi, V., Furuichi, T., *et al.* (1991) *Nature* **350,** 398–402.
29. Klugbauer, N., Lacinova, L., Marais, E., Hobom, M. & Hofmann, F. (1999) *J. Neurosci.* **19,** 684–691.
30. Hobom, M., Dai, S., Marais, E., Lacinova, L., Hofmann, F. & Klugbauer, N. (2000) *Eur. J. Neurosci.* **12,** 1217–1226.
31. Carman, C. V. & Springer, T. A. (2003) *Curr. Opin. Cell Biol.* **15,** 547–556.
32. Wang, M.-C., Collins, R., Ford, R. C., Berrow, N. S., Dolphin, A. C. & Kitmitto, A. (2004) *J. Biol. Chem.* **279,** 7159–7168.
33. Wolf, M., Eberhart, A., Glossmann, H., Striessnig, J. & Grigorieff, N. (2003) *J. Mol. Biol.* **332,** 171–182.
34. Wang, M. C., Dolphin, A. & Kitmitto, A. (2004) *FEBS Lett.* **564,** 245–250.
35. Wang, M.-C., Berrow, N. S., Ford, R. C., Dolphin, A. C. & Kitmitto, A. (2002) *J. Mol. Biol.* **323,** 85–98.
36. Passafaro, M., Clementi, F. & Sher, E. (1992) *J. Neurosci.* **12,** 3372–3379.

BIOCHEMISTRY